Solid State Communications 150 (2010) 1802–1806

Contents lists available at ScienceDirect

Solid State Communications

journal homepage: www.elsevier.com/locate/ssc

Short-range ordering state and cluster-glass behavior in electron-doped manganite $Y_{0.4}Ca_{0.6}MnO_3$

Langsheng Ling [a,*], Lei Zhang [a], Zhitao Zhang [b], Li Pi [b], Shun Tan [b], Yuheng Zhang [b]

[a] High Magnetic Field Laboratory, Chinese Academy of Sciences, Hefei 230031, People's Republic of China

[b] High Magnetic Field Laboratory, University of Science and Technology of China, Hefei 230026, People's Republic of China

ARTICLE INFO

Article history:
Received 11 May 2010
Received in revised form
5 July 2010
Accepted 6 July 2010
by E.G. Wang
Available online 14 July 2010

Keywords:
D. Order–disorder effects
D. Electronic transport

ABSTRACT

In this paper, we investigated the electrical and magnetic properties of electron-doped manganite $Y_{0.4}Ca_{0.6}MnO_3$ with a relatively small average cationic radius $\langle r_A\rangle$. The small $\langle r_A\rangle$ of the present system results in a short-range antiferromagnetic charge-ordering (AFM-CO) state in the manganite. With the decrease of temperature, a ferromagnetic super-exchange interaction begins to establish itself between the remaining disordered Mn ions after the formation of the short-range CO state. Then, a reentrant cluster-glass state originates from the frustration between the FM order in the clusters and the AFM interactions present in the background matrix.

1. Introduction

The manganites of ABO_3 type have attracted great attention from the researchers in recent years due to the fascinating properties such as colossal magnetoresistance (CMR), charge-ordering (CO), and the potential for applications [1]. Decades of research have allowed us to completely understand the full range of ordered phases that occur in the $R_{1-x}A_xMnO_3$ perovskites (R = La, Pr, Nd and A = Ca, Sr, Ba) [2]. For samples with $x \leqslant 0.5$, a complex competition occurs between ferromagnetic (FM), paramagnetic (PM), and antiferromagnetic (AFM) phases. In this regime, inhomogeneous phase separation (PS) gives rise to the well-known colossal magnetoresistance effect [3–5]. On the other hand, electron-doped manganites with $x \geqslant 0.5$ display orbital and charge-ordering with an antiferromagnetic ground state below the charge-ordering (CO) temperature T_{CO} [6,7].

Moreover, the properties of manganites are not only sensitive to the manganese valency, but also are strongly affected by the chemical factors such as average cationic radius $\langle r_A\rangle$ in the A-site [8–10] and the A-site cationic size mismatch [11,12] quantified by $\sigma^2 = \sum x_i r_i^2 - \langle r_A\rangle^2$ (x_i is the fractional occupancy of A-site ions, and r_i is the corresponding ionic radius) [11]. For instance, when the hole concentration is kept constant in the Mn^{3+}-rich FM compositions, it has been shown that the decrease of $\langle r_A\rangle$ tends to diminish the Mn–O–Mn angle, which consequently reduces the bandwidth (W) and the Curie temperature T_C [9]. In contrast, a small $\langle r_A\rangle$ value is required for the appearance of CMR in the Mn^{4+}-rich manganites [13]. Finally, whatever the $\langle r_A\rangle$ and the manganese valency are, the increase of σ^2 tends to suppress the magnetic interactions, FM or AFM, and destabilize the CO [11,12]. These behaviors show the great complexity of the relationships between the chemical factors ($\langle r_A\rangle$, σ^2, carrier nature, and concentration) and the magnetotransport properties of manganites.

Charge-ordering in the manganites is governed by the width of e_g band, which is directly determined by the weighted average radius of A-site cations $\langle r_A\rangle$, or the tolerance factor t. This is attributed to the fact that the distortion of Mn–O–Mn bond angle affects the transfer interaction of e_g conduction electrons (holes) [14]. A comparative study of the nature of the charge-ordered state has been carried out in hole-doped and electron-doped manganites, which revealed that the electronic structures of the two manganites have basic differences [15,16]. Electron–hole asymmetry is usually encountered in the rare-earth manganites and cuprate superconductors. This asymmetry has some unusual features, which is therefore worthy of investigation. Although early researchers have reported the relationship between T_{CO} and $\langle r_A\rangle$, they ignored the discrepancy in the behavior of M–T curves. The reason for these different magnetic behaviors and the physics involved have not been clarified. Further investigation of the A-site average radius will provide interesting insight. In this paper, we make a detailed investigation on the electrical and magnetic properties of the electron-doped manganite $Y_{0.4}Ca_{0.6}MnO_3$ which exhibits a charge-ordering state at relatively high T_{CO} with small $\langle r_A\rangle$. We hope to understand deeply the influence of relatively small $\langle r_A\rangle$ on the magnetic behavior of this charge-ordering system. The results indicate that the

* Corresponding author. Tel.: +86 551 5593619; fax: +86 551 5591149.
E-mail addresses: lsling@hmfl.ac.cn (L. Ling), zhangyh@ustc.edu.cn (Y. Zhang).

0038-1098/$ – see front matter © 2010 Elsevier Ltd. All rights reserved.
doi:10.1016/j.ssc.2010.07.010

severe distortion of MnO_6 octahedra in the present small-$\langle r_A \rangle$ system leads to the collapse of long-range ordering state and the formation of short-range ordering state. The reentrant cluster-glass state at low temperatures originates from the frustration between the FM order in the clusters and the AFM interactions present in the background matrix.

2. Experiment

Polycrystalline $Y_{0.4}Ca_{0.6}MnO_3$ sample was prepared by a traditional solid-state reaction method [17]. Stoichiometric quantities of high-purity oxide of the rare-earth Y_2O_3, $CaCO_3$, and MnO_2 were thoroughly mixed and ground, then preheated at 1173 K for 24 h. With intermediate grinding, they were reacted at 1473 K for 24 h. After the sample was pressed into pellets, a final sintering was carried out at 1573 K for 48 h. The structure and phase purity of as-prepared sample were checked by powder X-ray diffraction (XRD) using Cu K_α radiation at room temperature. The XRD pattern proves that the sample is single phase with orthorhombic perovskite structure. Magnetization measurements were performed by using a SQUID magnetometer (Quantum Design MPMS). Resistivity was measured by standard four-probe method. ESR measurements were also carried out on the sample by using a JES-FA200 spectrometer at 9.06 GHz.

3. Results and discussion

Fig. 1 shows the temperature dependence of magnetization, which was taken in warming-up processes with an applied field $H = 100$ Oe under zero-field-cooled (ZFC) and field-cooled (FC) condition. Here, peculiar magnetic behaviors can be observed. As seen in the inset of Fig. 1, the sample experiences a charge-ordering (CO) transition around 250 K. With further decreasing temperature, it is notable that the ZFC and FC magnetization curves start to separate from each other at a temperature around 110 K, where a strong irreversibility (difference between FC and ZFC magnetization) begins to develop, and the magnetic correlation between Mn ions appears. The steep drop of ZFC magnetization below 30 K results in an overall "λ"-shape magnetic behavior. This indicates the formation of a cluster-glass (CG) state. The magnetic behavior of $Y_{0.4}Ca_{0.6}MnO_3$ is different from that of the analogous compounds $Ln_{0.4}Ca_{0.6}MnO_3$ (Ln = La, Pr, Nd, Gd) [18,19] and $Y_{0.5}Ca_{0.5}MnO_3$ [20]. In these compounds, the system transfer into charge-ordering state around 270 K with decreasing temperature. However, there is no evidence of cluster-glass behavior at low temperatures. This difference may be resulted from the variation of radius and doping concentration of rare-earth ions.

The orthorhombic lattice distortion can be quantified by terms of the dimensionless index D which is defined as $D = \sum_{i=1}^{3} |a_i - a|/3a_i$ where $a_1 = a$, $a_2 = b$, and $a_3 = c/\sqrt{2}$, and $a = (abc/\sqrt{2})^{1/3}$. We performed structure analysis by using the Generalized Structure Analysis System (GSAS) [21]. The lattice parameters and index D are listed in Table 1. In the analogous compounds $Ln_{0.4}Ca_{0.6}MnO_3$ (Ln = La, Pr, Nd, Sm), the index D is about 0.3%. It is noteworthy that index D is 1.05% in $Y_{0.4}Ca_{0.6}MnO_3$ system, which is considerably larger than the analogous compounds. This result indicates the severe distortion of MnO_6 octahedra in the present small-$\langle r_A \rangle$ system.

The complex magnetic behaviors shown in Fig. 1 need to be investigated more carefully. First, the CO transition around 250 K should be verified. The micro-magnetism of the sample has been investigated through ESR spectra, which is shown in Fig. 2. At the temperature range between 130 and 370 K, only the paramagnetic signals with $g \approx 2$ have been detected in $Y_{0.4}Ca_{0.6}MnO_3$ [22,23]. With the decrease of temperature, the intensity of the PM

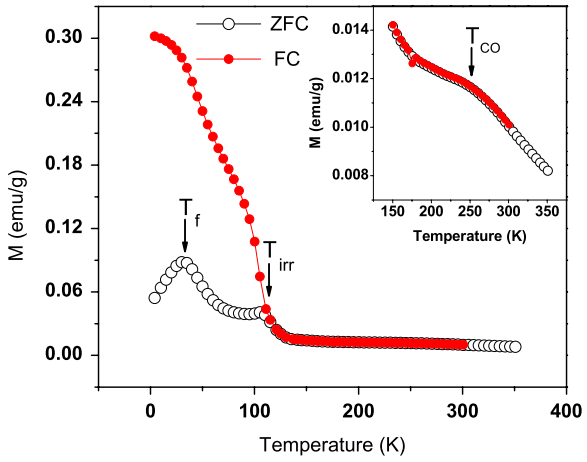

Fig. 1. Temperature dependence of magnetization (ZFC empty circle; FC solid circle) for $Y_{0.4}Ca_{0.6}MnO_3$. Inset shows the magnetization above 150 K.

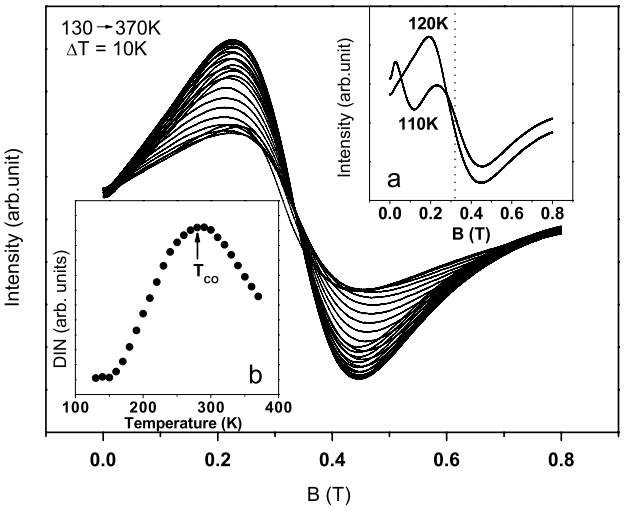

Fig. 2. Temperature dependence of ESR spectra. Inset(a): Low temperature ESR spectra. Dotted line locates at the resonance field of free electron; Inset(b): Temperature dependence of double integrated intensities (DIN).

signal increases first, then decreases after reaching a maximum. Since there is no ferromagnetic signal with $g > 2$, the above results indicate that the decrease of the intensity of the PM signal should be attributed to the formation of the AFM phase. In the temperature dependence of double integrated intensities (DIN) shown in Fig. 2(b), a broad peak occurs and the corresponding temperature is defined as T_{CO} [24]. In spite of the existence of the AFM phase, AFM signals have not been detected in the spectra. This may be due to the AFM coupling being too strong to be detected in ESR measurements.

As pointed out previously [19], in the present small-$\langle r_A \rangle$ system, the severe distortion of MnO_6 octahedra results in the collapse of the long-range ordering state and the formation of a local short-range ordering state. This result implies that the PM state at high temperatures does not transform into an AFM charge-ordering state completely at a temperature below T_{CO}. That is, only a fraction of Mn ions in the manganite establish the AFM coupling and transform into the AFM-CO phase. Thus there are a number of residual disordered Mn ions in the manganite, which dominate the magnetic behavior at low temperatures. Fig. 2(a) presents the ESR spectra measured at lower temperatures. At 120 K, the resonance line begins to deviate from the standard shape for a paramagnetic signal. Furthermore, at the lowest temperature 110 K, a FM signal with $g > 2$ manifest itself at the lower resonance field. This

indicates the FM phase develops at the temperature below 120 K, which in consistent with the magnetic behavior shown in M(T) curve. It also proves directly the existence of FM super-exchange interaction between the residual neighboring Mn^{3+} and Mn^{4+} ions.

At temperatures below 110 K, the ferromagnetic super-exchange interaction between the residual neighboring Mn^{3+} and Mn^{4+} ions takes place, which results in the rapid increase of magnetization and the strong irreversibility between the ZFC and FC curves. The temperature where bifurcation occurs is defined as the irreversibility temperature $T_{irr} \approx 110$ K. At 30 K, there is a peak in the ZFC curve. Then the magnetization decreases with temperature, while in the FC curve, the magnetization increases rapidly with the temperature decreasing from 110 to 4 K. This "λ"-shape magnetic behavior indicates the cluster-glass state which originates from the frustration between the FM order in the clusters with the AFM interactions present in the background matrix. Canonical spin-glass (SG) systems typically display a bifurcation of the ZFC and FC magnetization only very close to the SG freezing temperature T_f [25] with the FC curve almost flat whereas the ZFC magnetization drops at lower temperatures [26–28]. In the present case, however, the temperature T_{irr} is far above T_f. In some respects this resembles "cluster-glass" behavior as pointed out by several authors [29]. Furthermore, the difference between M_{FC} and M_{ZFC} is much larger in the cluster-glass phase compared to that in the spin-glass phase (corresponding to $La_{1-x}Sr_xCoO_3$ for $x < 0.2$) at sufficiently low temperatures, which indicates the presence of short-range ferromagnetic ordering within a cluster. Thus the conclusion can be drawn that the low temperature behavior indicates the cluster-glass state in the system.

Fig. 3 presents the temperature dependence of magnetization measured under different magnetic fields. The following points are observed: (1) The divergence between M_{FC} and M_{ZFC} at the temperature between T_{irr} and T_f becomes smaller with increasing magnetic fields, and eventually both are superposed with each other, exhibiting a typical PM behavior at a measuring field larger than 2000 Oe. This fact implies that whatever the cause of the irreversibility, the anisotropy field (which freezes the spins) is not large; (2) The cluster freezing temperature decreases with increasing magnetic fields. At the measuring field larger than 5000 Oe, the spins of cluster prefer to orient toward the direction of applied field rather than freeze randomly. These results reveal the fact that the long-range magnetic order is absent in $Y_{0.4}Ca_{0.6}MnO_3$ system.

The resistivity of $Y_{0.4}Ca_{0.6}MnO_3$ as a function of temperature recorded under zero magnetic field and 6 T is presented in Fig. 4(a). Generally speaking, the charge-ordering state in manganite is associated with insulating behavior. The resistivity is relatively small (about 10^{-2} Ω cm) at room temperature, but it rises rapidly with decreasing temperature and reaches 10^5 Ω cm at the lowest temperature measured. It also can be noticed that a magnetic field of 6 T has negligible effect on the resistivity. Thus, the short-range charge-ordering state shows less sensitivity to the magnetic field, and it may be melted at higher magnetic field (≫6 T). We further investigate the resistivity mechanism in the system. Usually a semiconductor-like transport behavior can be described by the thermal activation model or adiabatic small-polaron hopping model or variable-range hopping model. These three models are expressed as following:

$$\rho = \rho_0 exp(E_A/k_BT)$$
$$\rho = \rho_0 T exp(E_P/k_BT)$$
$$\rho = \rho_0 exp(E_{VRH}/k_BT)^{1/4}.$$

Here, ρ_0 is a pre-exponential factor. E_A, E_P, and E_{VRH} are the hopping energy for different models. As shown in Fig. 4(b)–(d), the resistivity is plotted as $\ln\rho$ versus T^{-1}, $\ln(\rho/T)$ versus T^{-1}, and $\ln\rho$ versus $T^{-1/4}$ respectively. It can be seen clearly that the low temperature resistivity can be well fitted according to the 3D variable-range hopping (VRH) model $\rho = \rho_0 exp(E_{VRH}/k_BT)^{1/4}$.

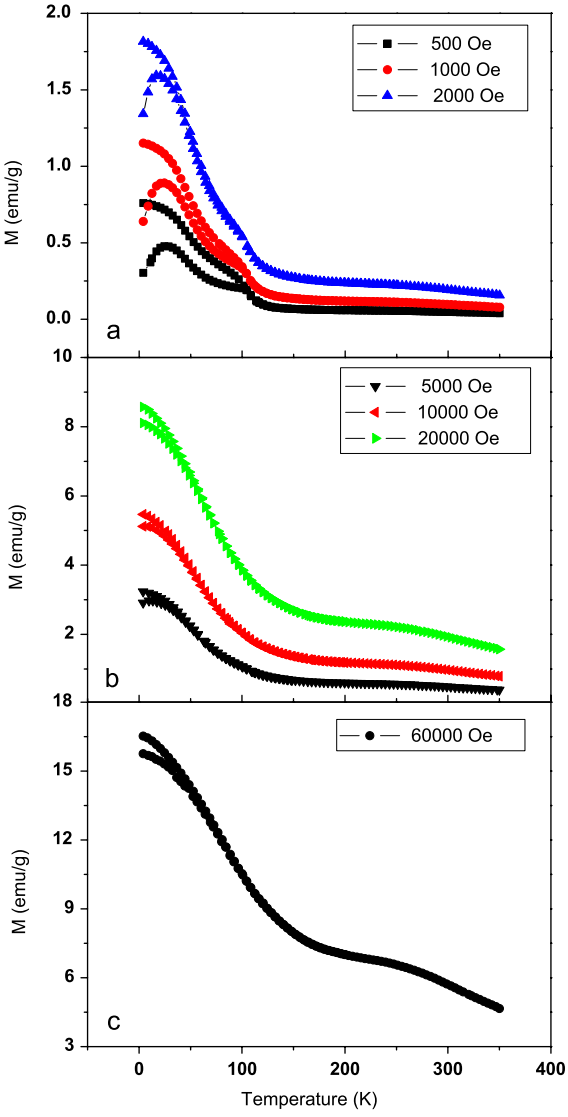

Fig. 3. Temperature dependence of magnetization measured under different fields.

Originally, the VRH theory was developed to explain electrical transport in doped semiconductors, where electrons are localized by potential fluctuations associated with the dopant as the small polarons [30,31]. In the present case, with decreasing temperature the system transfers into the short-range charge-ordering state. These short-range CO region distribute randomly in the system. In the CO region, the electrons are localized by the high potential barriers. Therefore, the thermal energy is not great enough to allow electrons to hop to their nearest neighbors. It is more favorable for the electrons to hop further to find a site with a smaller potential difference. Thus, variable-range hopping occurs. The low temperature transport behavior indicates further the short-range CO state.

We have summarized $\langle r_A\rangle$, σ^2, T_{CO} in Table 1. The weighted average radius of the A-site cations $\langle r_A\rangle$ ($\langle r_A\rangle = \sum x_i r_i$) and σ^2 ($\sigma^2 = \sum x_i r_i^2 - \langle r_A\rangle^2$) are calculated using nine-coordinated ionic radii given by Shannon [32]. It is noticeable that the T_{CO} values evaluated from different measurements are different from each other, which demonstrates the short-range character of the charge-ordering phase transition. It is well known that the σ^2 is used to define the size mismatch at A-site, and $\langle r_A\rangle$ directly

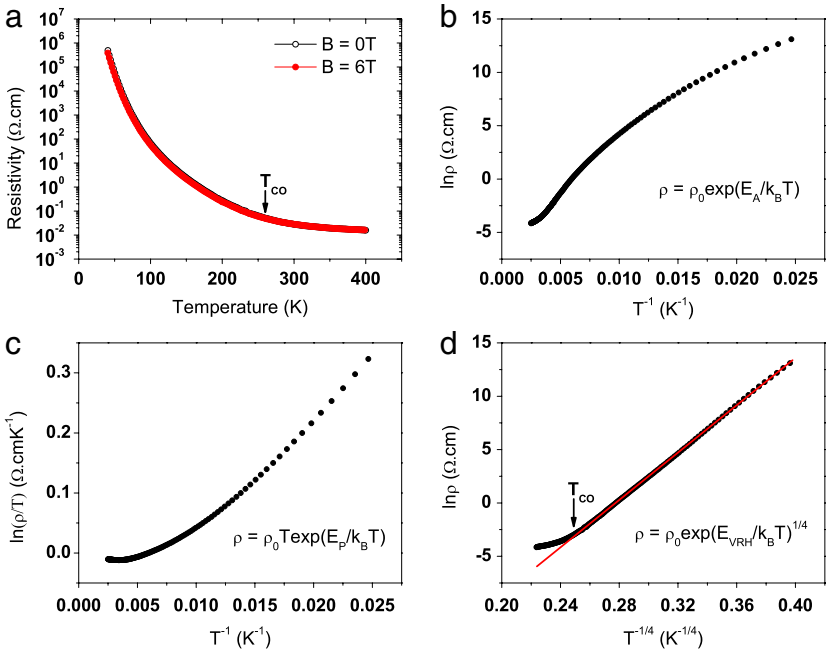

Fig. 4. (a) Temperature dependence of the resistivity of $Y_{0.4}Ca_{0.6}MnO_3$ measured under zero field and 6 T. (b) Resistivity plotted as ln ρ versus T^{-1}. (c) Resistivity plotted as $\ln(\rho/T)$ versus T^{-1}. (d) Resistivity plotted as ln ρ versus $T^{-1/4}$. The line is the linear fit to the data.

Table 1
$\langle r_A\rangle$, σ^2, lattice parameters, index D, and T_{CO} of $Y_{0.4}Ca_{0.6}MnO_3$ manganite.

$\langle r_A\rangle$ (Å)	σ^2 ($\times 10^{-4}$ Å^2)	a (Å)	b (Å)	c (Å)	D	T_{CO} (K)		
						M–T	ρ–T	ESR
1.1380	26.4600	5.2810	5.3961	7.4357	1.05%	250	260	280

affects the Mn–O–Mn angle, bandwidth W, and the average Mn–O distance in the manganites. The small $\langle r_A\rangle$ and large σ^2 in the present manganite weaken the hopping integral of e_g electrons and tend to facilitate the localization of separate Mn^{3+} and Mn^{4+} ions through the formation of polaron.

In order to get an insight into the cluster-glass state. The magnetic hysteresis loops shown in Fig. 5 were taken at 4 K when the sample was cooled down to 4 K under different fields from 200 Oe to 10 KOe. It can be seen clearly that the magnetic hysteresis loops shift in both horizontal and vertical directions. This result can be understood directly due to the fact that the spins of cluster are aligned to the field direction upon field cooling. When field cooled, the spins of cluster orient toward the direction of applied field. Furthermore, the cluster cannot rotate freely below the freezing temperature, so that the magnetization will not disappear with the applied field removed and a negative external field is needed to bring it back to zero. In the first loop cooled under 200 Oe all data are positive, since the applied field is too small to redirect the freezing spins. With the cooling field and measuring field increasing, more and more clusters are aligned to the applied field direction and the vertical and horizontal shifts become smaller at field of 10 KOe. The nature of this magnetic behavior is attributed to the freezing properties of the local anisotropy in the cluster-glass system [33].

To provide further evidence for the cluster-glass state, the ac magnetization has been measured as a function of temperature under different frequencies for an ac measuring field 3 Oe. The measured results do reveal the typical features of cluster-glass behavior. As shown in Fig. 6, there is a maximum at T_f in the ac magnetization, which shifts toward the higher temperatures with increasing frequency. Below the T_f, the magnitude of magnetization is frequency dependent, but it becomes independent of frequency at temperatures just above T_f. This fact supports our above

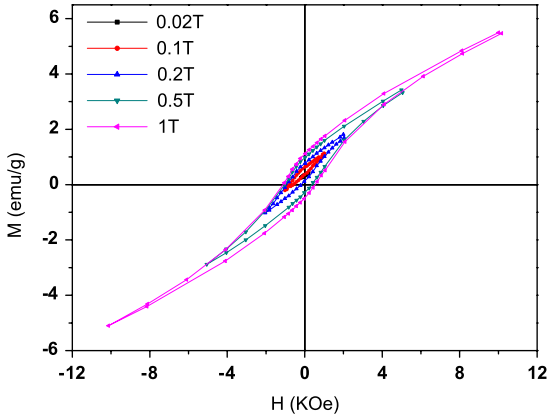

Fig. 5. Magnetic hysteresis loops taken at 4 K when the sample was cooled down to 4 K under different fields.

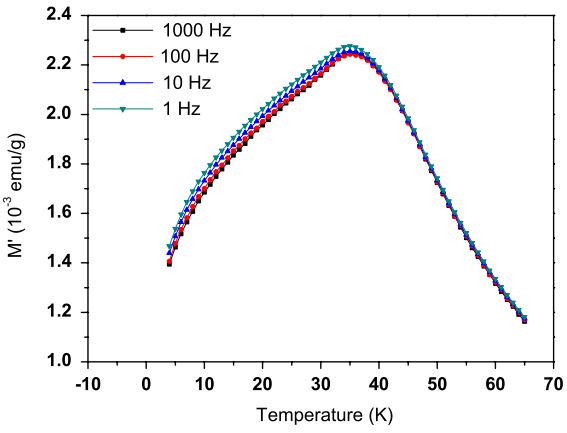

Fig. 6. Temperature dependence of ac magnetization. The data were recorded in an ac-field of 3 Oe with different frequencies.

argument on the cluster-glass state as the ground state at low temperatures. Fig. 7 shows the normalized long-time relaxation of the

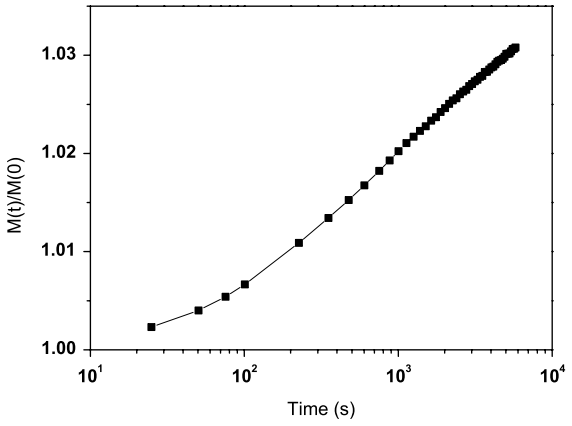

Fig. 7. Time dependence of the normalized magnetization M(t)/M(0) at 4 K, where M(0) is the magnetization value at the initial measured time. The sample was initially cooled down to 4 K, and then the magnetic field was applied. After the applied magnetic field was stable, the magnetic data were collected as a function of time. The time at which the first datum was taken is regarded as the initial time.

magnetization measured in a magnetic field 100 Oe at 4 K. It can be seen clearly that the magnetization increases monotonically with time even after 5×10^3 s. However, the relaxation is very slow which may attributed to the intrinsic magnetic frustration in the present system [34]. This fact is consistent with the cluster-glass behavior.

4. Conclusion

In this work we provide a detailed study of the magnetic and electrical properties of $Y_{0.4}Ca_{0.6}MnO_3$ composition. The effect of $\langle r_A \rangle$ is seen to be profound on the charge-ordering behavior of the manganite. The severe distortion of MnO_6 octahedra in the present small-$\langle r_A \rangle$ system results in the collapse of the long-range ordering state and the formation of a short-range ordering state. The irreversibility below 110 K originates from the ferromagnetic super-exchange interaction between remaining disordered Mn ions after the formation of short-range ordering state in the manganite. Finally, the cluster-glass state begins to manifest itself due to the frustration between the FM order in the clusters with the AFM interactions present in the background matrix.

Acknowledgements

This work is supported by the National Natural Science Foundation of China through Grant No. 10904149, Spark Foundation of Hefei Institute of Physical Science through Grant No. Y06CS61131, and the State Key Project of Fundamental Research, China, through Grant No. 2007CB925001.

References

[1] C.N.R. Rao, B. Raveau (Eds.), Colossal Magnetoresistance, World Scientific, Singapore, 1998.
[2] M.B. Salamon, M. Jaime, Rev. Modern Phys. 73 (2001) 583;
J.M.D. Coey, M. Viret, S. von Molnar, Adv. Phys. 48 (1999) 167.
[3] S. Jin, T.H. Tiefel, M. McCormack, R.A. Fastnacht, R. Ramesh, L.H. Chen, Science 264 (1994) 413.
[4] E. Dagotto, T. Hotta, A. Moreo, Phys. Rep. 344 (2001) 1.
[5] M. Fäth, S. Freisem, A.A. Menovsky, Y. Tomioka, J. Aarts, J.A. Mydosh, Science 285 (1999) 1540.
[6] Jeroen van den Brink, Giniyat Khaliullin, Daniel Khomskii, Phys. Rev. Lett. 83 (1999) 5118.
[7] P.G. Radaelli, D.E. Cox, M. Marezio, S.W. Cheong, Phys. Rev. B 55 (1997) 3015.
[8] R. Mahesh, R. Mahendiran, A.K. Raychaudhuri, C.N.R. Rao, J. Solid State Chem. 114 (1995) 297.
[9] H.Y. Hwang, S.W. Cheong, P.G. Radaelli, M. Marezio, B. Batlogg, Phys. Rev. Lett. 75 (1995) 914.
[10] A. Maignan, Ch. Simon, V. Caignaert, B. Raveau, Solid State Commun. 96 (1995) 623.
[11] L.M. Rodriguez-Martinez, J.P. Attfield, Phys. Rev. B 54 (1996) 15622.
[12] F. Damay, C. Martin, A. Maignan, B. Raveau, J. Appl. Phys. 82 (1997) 6181.
[13] A. Maignan, C. Martin, F. Damay, B. Raveau, Chem. Mater. 10 (1998) 950.
[14] T. Vogt, A.K. Cheetham, R. Mahendiran, A.K. Raychaudhuri, R. Mahesh, C.N.R. Rao, Phys. Rev. B 54 (1996) 15303.
[15] S. Parashar, K.V. Sarathy, P.V. Vanitha, A.R. Raju, C.N.R. Rao, J. Phys. Chem. Solids 62 (2001) 1387.
[16] K.V. Sarathy, P.V. Vanitha, R. Seshadri, A.K. Cheetham, C.N.R. Rao, Chem. Mater. 13 (2001) 787.
[17] J. Fan, L. Ling, B. Hong, L. Pi, Y. Zhang, J. Magn. Magn. Mater. 321 (2009) 2838.
[18] L. Ling, J. Fan, L. Pi, Y. Ying, S. Tan, Y. Zhang, J. Phys.: Condens. Matter 20 (2008) 125214.
[19] L. Ling, J. Fan, L. Pi, Y. Ying, S. Tan, Y. Zhang, Solid State Commun. 144 (2007) 189.
[20] A. Arulraj, R. Gundakaram, A. Biswas, N. Gayathri, A.K. Raychaudhuri, C.N.R. Rao, J. Phys.: Condens. Matter 10 (1998) 4447.
[21] B.H. Toby, J. Appl. Cryst. 34 (2001) 210.
[22] C. Autret, M. Gervais, F. Gervais, N. Raimboux, P. Simon, Solid State Sci. 6 (2004) 815.
[23] R. Gupta, J.P. Joshi, S.V. Bhat, A.K. Sood, C.N.R. Rao, J. Phys.: Condens. Matter 12 (2000) 6919.
[24] C. Autret, M. Gervais, M. Zaghrioui, S. Roger, F. Gervais, N. Raimboux, P. Simon, Eur. Phys. J. B 47 (2005) 207.
[25] J.A. Mydosh (Ed.), Spin-Glasses: An Experimental Introduction, Taylor and Francis, London, 1993.
[26] A. Sundaresan, A. Maignan, B. Raveau, Phys. Rev. B 55 (1997) 5596.
[27] J.M. De Teresa, M.R. Ibarra, J. Garcia, J. Blasco, C. Ritter, P.A. Algarabel, C. Marquina, A. del Moral, Phys. Rev. Lett. 76 (1996) 3392.
[28] A. Maignan, C. Martin, G. Van Tendeloo, M. Hervieu, B. Raveau, Phys. Rev. B 60 (1999) 15214.
[29] S. Mukherjee, R. Ranganathan, P.S. Anilkumar, P.A. Joy, Phys. Rev. B 54 (1996) 9267.
[30] N.F. Mott (Ed.), Metal–insulator Transitions, Taylor and Francis, London, 1985.
[31] N.F. Mott, E.A. Davies (Eds.), Electronic Processes in Noncrystalline Materials, Oxford University Press, Oxford, 1971.
[32] R.D. Shannon, Acta Crystallogr. A 32 (1976) 751.
[33] W.J. Luo, F.W. Wang, Appl. Phys. Lett. 90 (2007) 162515.
[34] W.R. Chen, F.C. Zhang, J. Miao, B. Xu, L.X. Cao, X.G. Qiu, B.R. Zhao, J. Phys.: Condens. Matter 17 (2005) 8029.